Available online at www.sciencedirect.com
ScienceDirect
Ceramics International 35 (2009) 2401–2408
CERAMICS INTERNATIONAL
www.elsevier.com/locate/ceramint

Synthesis, microstructure and optical characterization of zirconium oxide nanostructures

Latha Kumari [a], G.H. Du [a], W.Z. Li [a,*], R. Selva Vennila [b], S.K. Saxena [b], D.Z. Wang [c]

[a] Department of Physics, Florida International University, Miami, FL 33199, United States
[b] Center for the Study of Matter at Extreme Conditions, Florida International University, Miami, FL 33199, United States
[c] Department of Physics, Boston College, Chestnut Hill, MA 02467, United States

Received 11 December 2008; received in revised form 29 December 2008; accepted 2 February 2009
Available online 25 February 2009

Abstract

Zirconium oxide (ZrO_2) nanostructures were synthesized by hydrothermal route. Surface morphology analysis depicts the formation of the nanobars and hexagonal-shaped nanodiscs at different synthesis conditions. The structural analysis confirms that the as-synthesized ZrO_2 product is of pure monoclinic phase (m-ZrO_2) with crystallite size of about 25 nm. The product consists of monodispersed nanoparticles of uniform composition, high purity, and crystallinity. The Raman spectra are quantitatively analyzed and the observed peaks are attributed to various vibration modes of the m-ZrO_2. The UV–vis absorption spectrum showed a strong absorption peak at about 292 nm and the estimated optical band gap was around 3.57 eV. Photoluminescence (PL) spectrum of ZrO_2 nanostructure showed a strong and broad emission peak at around 410 nm at room temperature, which can be attributed to the ionized oxygen vacancy in the material.

Keywords: A. Powder: chemical preparation; B. Electron microscopy; C. Optical properties; D. ZrO_2

1. Introduction

Zirconium oxide (ZrO_2) has attracted considerable attention because of its diverse practical applications in fuel-cell technology [1], as a catalyst or catalyst support [2], oxygen sensor [3], protective coating for optical mirrors and filters [4], nanoelectronic devices, thermal-barrier coatings [5], ceramic biomaterial [6], and thermoluminescence UV dosimeter [7]. ZrO_2 nanostructures are of significant current interest in preparing piezoelectric, electrooptic, dielectric, and nanocomposite materials [8–10]. ZrO_2 is classified as a wide band gap semiconductor and tends to become more conductive with increasing temperatures. The crystal structure of ZrO_2 significantly influences its physical properties. Even the performance of the ZrO_2-based devices considerably depends on the crystal structure of ZrO_2. Pure ZrO_2 exists in three polymorphic phases at different temperatures: monoclinic, tetragonal, and cubic. At very high temperatures (>2370 °C) the material has a cubic structure. At intermediate temperatures (1150–2370 °C) it has a tetragonal structure. At low temperatures (below 1150 °C) the material transforms to the monoclinic structure which is a thermodynamically stable phase [11].

ZrO_2 optical properties [12], and especially photoluminescence (PL) properties have been seldom reported, although PL has already been observed in a ZrO_2 sol and nanoparticle systems [13]. There has been an increasing interest for the application of nanoparticles to photonics systems due to their enhanced luminescent properties, which exists due to their small size [14]. Recently, it has been demonstrated that wide-band gap oxide nanostructures with short-wavelength PL emission may be used as compact disc read-heads [15]. ZrO_2 powders with nanostructured particles have been synthesized by various techniques [16,17]. The successful syntheses of ZrO_2 nanotubes and nanofibers by direct electrochemical anodization [18] and electrospinning [19] have been reported. The template method has proven to be a versatile approach for preparing ordered nanotubes and nanowires [20,21]. Hydrothermal route is one of the most extensively employed techniques in the synthesis of metal oxide nanostructures

* Corresponding author. Tel.: +1 305 348 7257; fax: +1 305 348 6700.
E-mail address: Wenzhi.Li@fiu.edu (W.Z. Li).

0272-8842/$36.00
doi:10.1016/j.ceramint.2009.02.007

[22]. The hydrothermal method has many advantages, for example, a highly homogeneous crystalline product can be obtained directly at a relatively lower reaction temperature (<150 °C); it favors a decrease in agglomeration between particles, narrow particles size distribution, phase homogeneity, uniform composition, high product purity and controlled particle morphology [23].

In the present work, we discuss the synthesis of ZrO_2 nanostructures by hydrothermal method using zirconyl nitratre as a precursor at higher hydrolysis temperature (>200 °C), which is seldom reported [24]. We present the synthesis of pure m-ZrO_2 nanostructures with controlled morphology and high crystallinity. Structural analysis of the nanostructures is performed by transmission electron microscopy and X-ray diffractometry techniques. Raman spectral analysis and the vibration mode assignment of the nanostructures are discussed. UV–vis absorption and photoluminescence spectroscopic properties are also investigated.

2. Experimental

2.1. Synthesis of ZrO_2 nanomaterials

ZrO_2 nanostructures were synthesized by a simple hydrothermal route. Zirconyl nitrate hydrate ($ZrO(NO_3)_2{\cdot}xH_2O$) and sodium hydroxide (NaOH) were used as the starting materials for the nanostructure synthesis. All the chemicals were of analytical grade (Fisher scientific) and used without further purification. The detailed experimental procedure is discussed elsewhere [25]. For the synthesis of ZrO_2 nanostructures, 0.5 M $ZrO(NO_3)_2{\cdot}xH_2O$ and 5 M NaOH were mixed together and sonicated for 30 min to a obtain homogeneous mixture. Later, 10 mL of the above solution was loaded into a 20 mL Teflon-lined autoclave with 2 mL of absolute ethanol. Finally, the autoclave was sealed and maintained at 250 °C for 3 h (hydrothermal treatment time, t_H). Similar procedure was used to synthesize ZrO_2 product at 250 °C for t_H = 24 and 42 h. The autoclave was then allowed to cool down to room temperature naturally. The precipitate was filtered off, washed with absolute ethanol and distilled water several times, and then dried in air at 80 °C for 1 h. The white colored product so processed was later used for various characterizations.

2.2. Structural characterization

Surface morphology and chemical composition of the ZrO_2 nanostructures were analyzed by field emission scanning electron microscope (FESEM, JEOL JSM-6330F, 15 kV) equipped with energy-dispersive X-ray spectroscopy (EDS, Thermo electron Corp.). Transmission electron microscopy (TEM) analysis was performed with a JEOL-2010 apparatus operated at an accelerating voltage of 200 kV. For TEM analysis, the product was ultrasonically dispersed in ethanol and then spread on the carbon-coated copper grids. Structural analysis was carried out by employing an X-ray diffractometer (D-8 Bruker-AXS) equipped with a Cu K_α radiation source (λ = 1.5406 Å) and a two-dimensional area detector. Raman spectra of ZrO_2 nanostructures were obtained from a Spectra Physics Laser Inc. apparatus with 514 nm incident photons from an Ar ion laser operated at a maximum power of 15 mW and equipped with Peltier-cooled CCD detector (Kaiser Optical systems). The Raman spectra have a resolution of 4 cm^{-1}. UV–vis spectrum was obtained from Perkin-Elmer Lambda 900 UV–vis/NIR spectrometer and the photoluminescence spectrum was recorded from SPEX FluoroLog spectrofluorometer (Horiba, Jobin Yvon). For the spectroscopic analysis, nanomaterials were dispersed in NaOH solution at room temperature and taken in quartz cell.

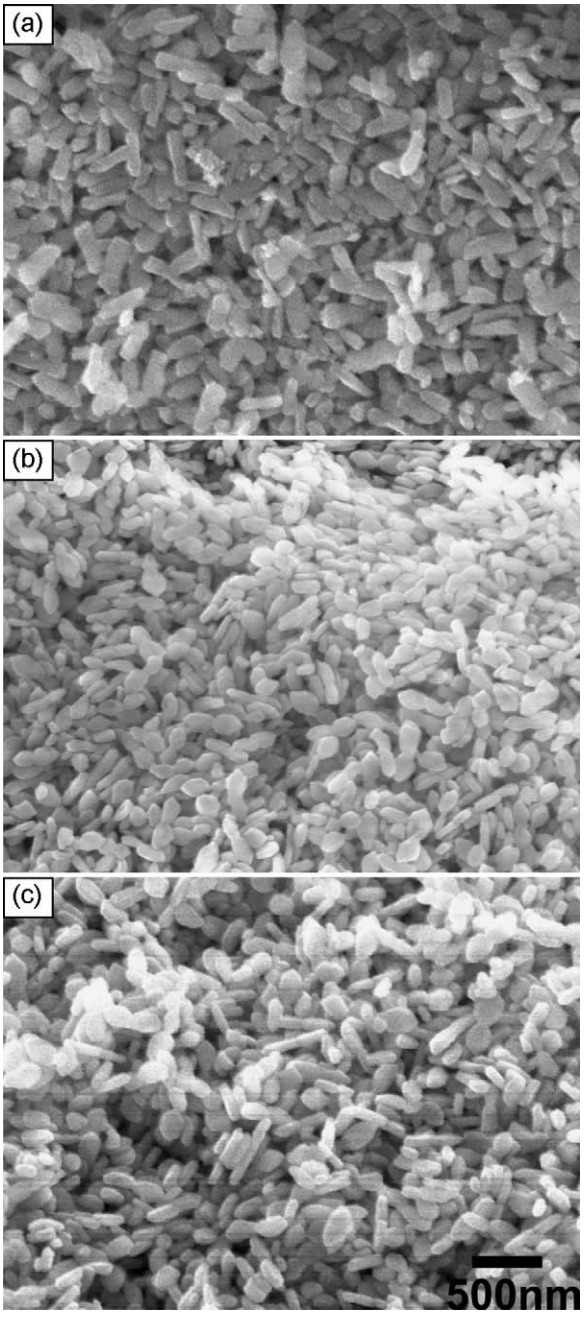

Fig. 1. FESEM images of the as-synthesized ZrO_2 product at 250 °C for (a) 3 h, (b) 24 h, and (c) 42 h.

3. Results and discussion

3.1. Microstructure analysis

FESEM images of the ZrO_2 nanostructures synthesized at hydrothermal treatment temperature of 250 °C for t_H = 3, 24 and 42 h are shown in Fig. 1(a)–(c). ZrO_2 product prepared for 3 h consists of nanobars of about 100–120 nm in width and 350–450 nm in length. However, the sample on large scale depicts monodispersed nanobars with controlled morphology, which is significant in samples synthesized by hydrothermal route [23]. Apart from the well resolved nanobars, the sample is found to be comprised of un-reacted material (not shown), which is also confirmed from the existence of traces of 'Na' as indicated by the EDS spectra in inset (i) of Fig. 2(b). A narrow size distribution of the hexahedron-like nanodiscs of ~150 nm in width and ~40 nm in thickness is obtained in samples prepared at 24 and 42 h, as shown in Fig. 1(b) and (c), respectively. However, no appreciable change in the shape of the nanodiscs prepared for 42 h is observed as compared to the nanodiscs prepared for 24 h, except slight increase in size of about 7 nm. ZrO_2 nanodiscs consist of only two elements 'O' and 'Zr' with approximate atomic concentration ratio of 2:1, which is determined by EDS spectra in the inset (ii) of Fig. 2(b) for the sample synthesized for 24 h. Similar atomic concentrations were also obtained for ZrO_2 sample synthesized for 42 h. FESEM images and EDS spectra of nanocrystalline ZrO_2 samples confirm the synthesis of highly monodispersed nanodiscs with controlled surface morphology, homogeneous phase, and uniform composition [23].

Fig. 2(a) represents a high-magnification FESEM image of the hexahedron-shaped ZrO_2 nanodiscs prepared for 24 h. Albeit, the ZrO_2 sample consists of large amount of hexahedron-like nanodiscs, the product also shows the tendency to grow nanorods of about 130–300 nm in width and varying length of 1.2–2.3 μm at different regions (Fig. 2(c) and (d)). But, the nanorods are formed very sparsely, along with the large-scale synthesis of hexagonal-shaped nanodiscs. Most of the earlier reports on the synthesis of ZrO_2 nanostructures by hydrothermal route suggested the growth of nanoparticles of various sizes and shapes [24,26]. However, the regular shaped ZrO_2 nanostructures synthesized by the above method are seldom reported. At present, we have no explanation for the formation of the nanorods. In future, we aim at optimizing the preparation conditions for the large-scale synthesis of nanorods or nanowires by hydrothermal technique. Our earlier report on the synthesis of ZrO_2 nanostructures at 200 °C presents rice grain-like and spindle-like growth of ZrO_2 nanomaterials at various hydrothermal treatment times [25]. Hence, by varying the hydrothermal synthesis parameters (temperature, pressure, duration, concentration, and the pH of precursor solutions), one can achieve the targeted microstructure, morphology, and phase composition of nanocrystalline hydrothermal products.

3.2. X-ray diffraction analysis

XRD profiles of ZrO_2 nanostructures synthesized at 250 °C for t_H = 3, 24 and 42 h are respectively shown in Fig. 3. The diffraction peaks in the spectra are indexed as monoclinic

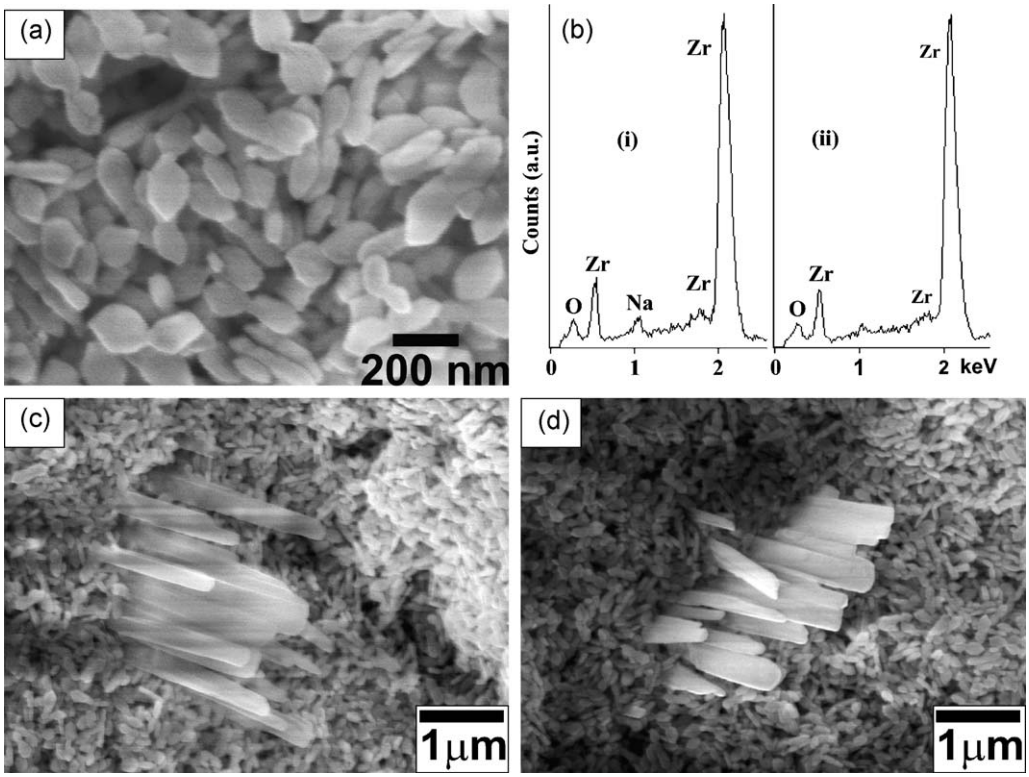

Fig. 2. (a) High-magnification FESEM image of the as-synthesized ZrO_2 nanodiscs at 250 °C for 24 h, (b) EDS spectra of ZrO_2 sample synthesized for (i) 3 h and (ii) 24 h. (c) and (d) present the tendency of ZrO_2 nanodiscs to grow into nanorods at different regions.

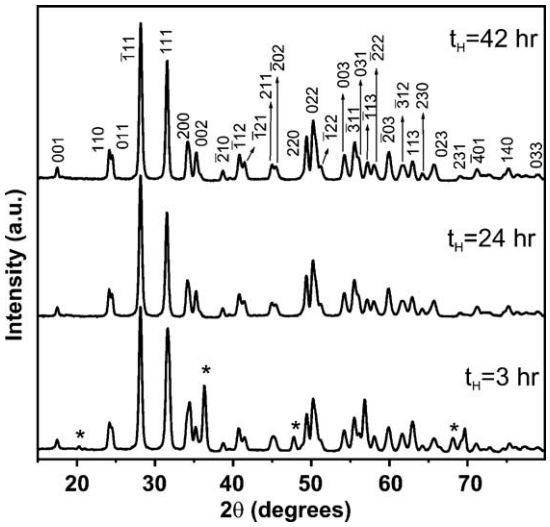

Fig. 3. XRD profiles of as-synthesized ZrO_2 product at 250 °C for t_H = 3, 24 and 42 h, respectively. The diffraction peaks are attributed to m-ZrO_2 standard data and are marked accordingly. Four new XRD peaks of ZrO_2 product for t_H = 3 h are marked with '*' and can be assigned to traces of impurity in the sample.

(baddeleyite) ZrO_2 with lattice constants, $a = 0.5313$ nm, $b = 0.5213$, $c = 0.5147$ nm and $\beta = 99.22°$ and are in good agreement with those of the standard data (JCPDS 37-1484) [26,27]. Almost all the diffraction peaks with similar relative intensity as suggested in the standard data are observed in the experimental XRD pattern and are significantly sharp, hence confirming the purity and high crystallinity of the synthesized ZrO_2 samples. Moreover, all the prominent peaks with sufficient peak intensity are indexed as shown in the Fig. 3.

The strongest diffraction peak at around 28.2° corresponds to the ($\bar{1}$ 1 1) plane. All the peaks with the same intensity, full width half maximum, and 2θ values are repeated in the XRD spectra of the samples prepared for t_H = 24 and 42 h (Fig. 3), except the sample synthesized for t_H = 3 h shows some dissimilarities in the spectra with respect to the other two samples. The most observable change in the XRD pattern for sample synthesized at t_H = 3 h is the existence of four new sharp peaks at around 20.3°, 36.3°, 47.8° and 68.2°, as indicated by the asterisks in Fig. 3. The three peaks at 36.3°, 47.8° and 68.2° can be attributed to the non-stoichiometric zirconium compound $ZrO_{0.27}$ (JCPDS 89-2340). A significant peak shift is observed for some of the peaks for t_H = 3 h ZrO_2 sample as compared with the ZrO_2 samples of t_H = 24 and 42 h, indicating the occurrence of stress or slight lattice distortions in the t_H = 3 h ZrO_2 sample. All these disparities in the ZrO_2 samples of t_H = 3 h arise due to the impurity in the synthesized product owing to the short hydrothermal treatment time, which is not sufficient enough for complete hydrothermal reaction to take place. This observation also supports the EDAX results, where the traces of element, 'Na' are still noticed in the synthesized product. The crystallite size of the ZrO_2 samples of t_H = 3, 24 and 42 h is determined by using Scherer's formula corresponding to the full width at half maximum of the ($\bar{1}$ 1 1) dominant peak and are found to be about 25 ± 1 nm.

For most of the reported ZrO_2 samples synthesized by hydrothermal techniques, the as-synthesized products are of mainly tetragonal or cubic or mixed phases [24,26,27] and they attain monoclinic phase only after calcination or annealing at higher temperatures (>1000 °C) [27]. The formation of the nanostructured ZrO_2 with single and pure monoclinic crystalline phase reported in our work signifies the importance of the present synthesis technique in obtaining ZrO_2 nanoparticles with uniform crystallite sizes, high purity, uniform composition and high crystallinity [23].

3.3. Crystal structure analysis by TEM

Further, the structural information of the ZrO_2 nanostructures is also studied by the TEM, high resolution TEM (HRTEM), and selected area electron diffraction (SAED). Fig. 4 represents the TEM image of ZrO_2 product showing both the hexahedron-shaped nanodiscs and flat nanorods, hence supporting our claim in the FESEM analysis. As seen in the TEM image, the sample consists of nanorods of about 100 nm wide and 425 nm long. It also presents nanodiscs of width varying between 100 nm and 150 nm. The growth direction of the ZrO_2 nanostructures follows along the [1 1 1] direction [28] as indicated in Fig. 4. The regions marked with boxes, A and B indicate the areas in which the HRTEM images of the nanodisc and nanorod were obtained, respectively.

The HRTEM images of ZrO_2 nanostructures in the form of hexahedron-like nanodiscs and nanorods are shown in Fig. 5(a) and (b) corresponding to the regions marked as A and B, respectively in Fig. 4. The HRTEM images show well resolved lattice fringes indicating the single crystalline nature and high crystallinity of the synthesized product. The lattice fringes are of equidistance and clear all along the length of the nanorods

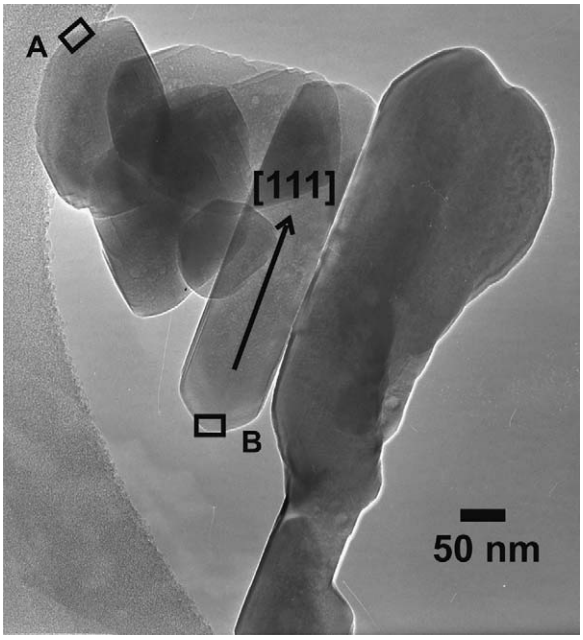

Fig. 4. TEM image of the as-synthesized ZrO_2 sample at 250 °C for 24 h, indicating both nanodiscs and nanorods. The growth of nanorod and nanodiscs is marked along [1 1 1] direction. Two rectangular open boxes marked as A and B on nanodiscs and nanorods respectively correspond to the regions at which HRTEM images are taken.

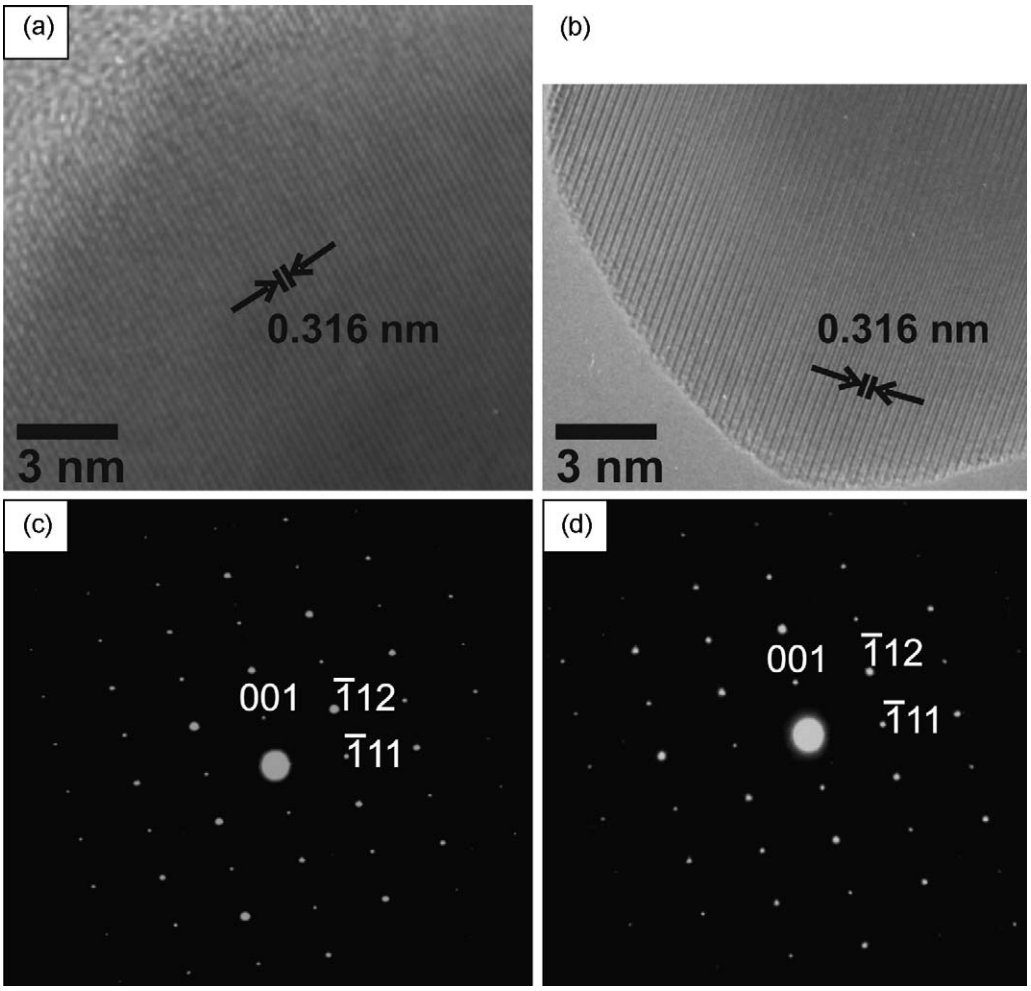

Fig. 5. HRTEM images of ZrO_2 nanodisc (a) and nanorod (b) obtained at the regions indicated as A and B respectively in Fig. 4. The discrete lattice fringes separated by 0.316 nm are observed in (a) and (b) corresponding to the $(\bar{1}\,1\,1)$ plane of m-ZrO_2. SAED pattern of ZrO_2 nanodisc (c) and nanorod (d) is shown and the respective diffraction spots are indexed.

and nanodiscs, without any lattice mismatch. These fringes are separated by 0.316 nm, which agrees well with the interplanar spacing corresponding to the $(\bar{1}\,1\,1)$ plane of m-ZrO_2. The clear spots in the SAED pattern (Fig. 5(c) and (d)) are indexed to (0 0 1), $(\bar{1}\,1\,2)$ and $(\bar{1}\,1\,1)$ planes, which can be attributed to the m-ZrO_2. Both the nanodiscs and nanorods show similar HRTEM images and SAED patterns, hence confirming the growth uniformity of the ZrO_2 product to form various nanostructures under the same synthesis conditions. The equally spaced reflections in the SAED pattern and lattice fringes correspond to the lattice planes of bulk m-ZrO_2, hence suggesting the purity and high crystallinity of the synthesized ZrO_2 product.

3.4. Raman spectroscopy

Raman spectroscopy is a nondestructive experimental technique for probing the vibrational and structural properties of materials. It is also recognized as a powerful tool to identify different polymorphs of metal oxides. From a group theory analysis, m-ZrO_2 is expected to have 18 ($9A_g + 9B_g$) Raman active modes [29]. According to Quintard et al. [30], owing to the low symmetry of the atomic positions and the large difference between the masses of oxygen and zirconium in ZrO_2, in the Raman spectra the low-frequency part would represent the g-combinations of Zirconium displacement and the rest of the spectra represent the g-combinations of oxygen atomic displacement. However, none of the previous works reported all the theoretically predicted 18 Raman bands. Experimentally, altogether 14 Raman bands have been identified and the different vibration modes are assigned [30,31]. Previous work by Ishigame and Sakurai [31] reported the mode assignments of m-ZrO_2 from the polarization Raman spectra of ZrO_2 single crystals.

Raman spectra of ZrO_2 nanostructures synthesized at 250 °C for $t_H = 3$, 24 and 42 h are shown in Fig. 6 and the corresponding Raman band parameters are listed in Table 1. These spectra confirm that the as-synthesized product is of monoclinic phase, which also supports the XRD analysis. The monoclinic sample presents very well defined peaks, and the intense peaks are located at 178, 189 and 476 cm^{-1} (characteristic peak of monoclinic phase) [30]. Raman spectra of the ZrO_2 samples show total 14 vibrations modes corresponding to the monoclinic phase. Most of the Raman

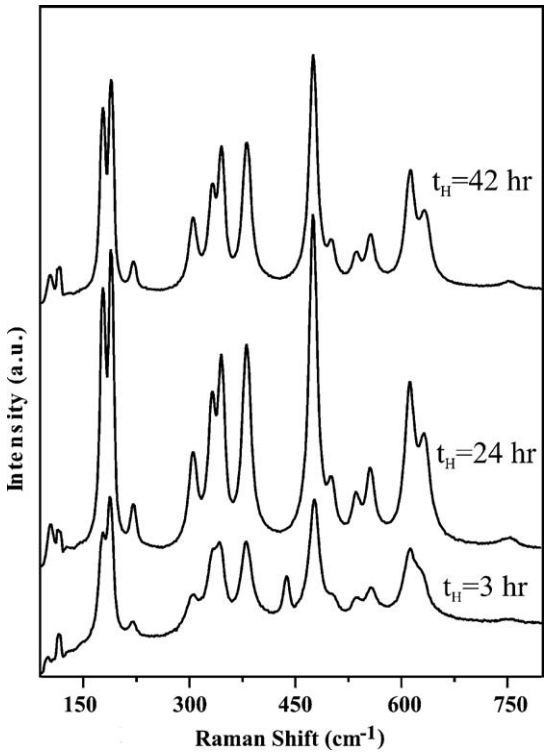

Fig. 6. Raman spectra of the as-synthesized ZrO_2 product at 250 °C for t_H = 3, 24 and 42 h, respectively.

lines were easily observable for both A_g and B_g conditions, but only one of the Raman signals (178 cm^{-1}) has been interpreted as an $A_g + B_g$ superposition [30,31]. Thus, the number of the observed vibrations is found to be 15. Additionally, three bands at 115, 118 (doublets) and 753 cm^{-1} have been observed in the Raman spectra of the ZrO_2 sample; these bands were described as the fundamental modes and taken into account to complete the list of Raman-active vibrations of m-ZrO_2 [32]. Among the 17 observed Raman peaks (Table 1), except the peaks at 115 and 118 all other bands are assigned to (O–O), (Zr–O) and (Zr–Zr) phonon vibration modes [32]. Earlier report by Anastassakis et al. [29] indicated that the broad band at 760 cm^{-1} can be assigned to a second-order process (overtone scattering) and the band at 105 cm^{-1} is a doublet. Barberis et al. [33] subjected the as-synthesized tetragonal powder to annealing at 900 °C under O_2/H_2O mixture to obtain monoclinic powder with 14 Raman peaks (extra peak at 158 cm^{-1}) attributed to m-ZrO_2. However, in the present work, as-synthesized ZrO_2 product is of pure monoclinic phase.

Raman spectra in Fig. 6 have been plotted on the same intensity scale, from which we can suggest that the intensity of the Raman bands increases drastically with the increase of the hydrothermal treatment time from t_H = 3–24 h, but decreases slightly with the further increase of the treatment time to t_H = 42 h. However, the number of Raman bands observed for all the spectra are the same, except for the sample synthesized for t_H = 3 h showing an extra peak at about 438 cm^{-1} with full width half maximum (FWHM) of 8 cm^{-1} which arises due to incomplete reaction. The Raman bands at 178, 306, 334, 346, 501 and 633 cm^{-1} for sample synthesized for t_H = 3 h are not well resolved (having shoulder-like peaks) with respect to the adjacent peak and as compared to those of samples synthesized for t_H = 24 and 42 h, hence suggesting the incomplete reaction for t_H = 3 h. The Raman band parameters in Table 1 show small variation in peak position and width for as-synthesized samples at various t_H values. As-synthesized ZrO_2 sample (t_H = 24 h) annealed at 400 °C for 3 h does not depict any appreciable change in peak position (not shown) and width, or phase transition as compared to that of the as-synthesized material. This result infers that the ZrO_2 nanostructures synthesized at 250 °C for 24 h or 42 h attains saturation and hence no change in the properties of these materials can be attained with further annealing. The above statement also has evidences from

Table 1
Raman peak positions, widths and vibration mode attribution of the monoclinic ZrO_2 synthesized at 250 °C for various hydrothermal treatment time (t_H).

Peak	Peak position (cm^{-1})			Peak width (FWHM) (cm^{-1})			Mode attribution	
	t_H = 3 h	t_H = 24 h	t_H = 42 h	t_H = 3 h	t_H = 24 h	t_H = 42 h		
1	102	104	103	4	8	7	A_g [a]	(O–O) [b]
2	115	114	114	n/a	n/a	n/a	–	–
3	118	117	117	n/a	n/a	n/a	–	–
4	n/a	179	178	n/a	9	11	$A_g + B_g$	(Zr–Zr)
5	185	190	189	5	6	7	A_g	(Zr–Zr)
6	219	221	221	12	8	8	B_g	(Zr–Zr)
7	306	306	306	n/a	9	8	A_g	(Zr–O)
8	n/a	334	334	n/a	5	6	B_g	(Zr–Zr)
9	n/a	346	346	n/a	7	7	A_g	(Zr–O)
10	381	382	382	13	11	11	B_g	(O–O)
11	477	476	476	12	10	10	A_g	(O–O)
12	n/a	501	501	n/a	11	11	B_g	(O–O)
13	538	538	537	7	5	6	B_g	(O–O)
14	557	557	557	11	9	9	A_g	(O–O)
15	613	614	614	8	8	8	B_g	(O–O)
16	n/a	633	633	n/a	7	11	A_g (O–O)	(O–O)
17	753	754	753	n/a	n/a	n/a	–	–

[a] Ref. [31].
[b] Ref. [33].

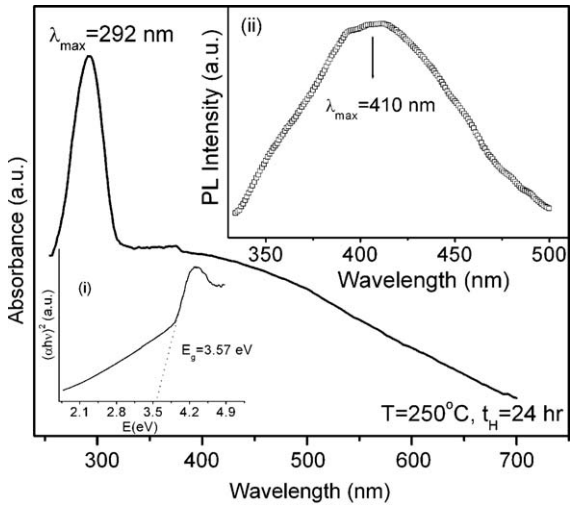

Fig. 7. UV–vis spectrum of ZrO_2 nanomaterial synthesized at 250 °C for 24 h, at room temperature. Inset (i) is $(\alpha h\gamma)^2$ vs. *energy* plot, depicting the optical band gap of about 3.57 eV and inset (ii) is the room temperature PL emission spectrum of the ZrO_2 nanostructure excited with light of wavelength 290 nm.

FESEM images and XRD profiles (not shown). To the best of our knowledge, there are no reports discussing the synthesis of ZrO_2 product by hydrothermal route which can present almost all the Raman peaks attributed to the pure m-ZrO_2 [30,32] as observed in the present work.

3.5. UV–vis absorption and photoluminescence spectroscopy

UV–vis absorption spectrum recorded for ZrO_2 nanomaterial synthesized at 250 °C for 24 h, in the wavelength range 250–700 nm is as shown in Fig. 7. The spectrum shows a sharp and prominent absorption band with maximum at around 292 nm (4.25 eV in photon energy) which can arise due to the transition between valence band to conduction band [34]. However, the absorption peak for the ZrO_2 nanostructure in the UV-region is at lower energy as compared to the previous report on the optical band gap for bulk ZrO_2 (5.0 eV) [13]. This indicates that there is still contribution from extrinsic states towards the absorption in this region. Apart from the strong absorption peak, a broad and weak peak centered at around 500 nm (∼2.5 eV in photon energy) exists. The weak absorption in the near UV and visible region is expected to arise from transitions involving extrinsic states such as surface trap states or defect states or impurities [13]. The direct band gap energy can be determined by plotting $(\alpha h\gamma)^2$ vs. energy (inset (i) of Fig. 7), where α is the absorption coefficient and $h\gamma$ is the photon energy. The optical band gap determined for the ZrO_2 nanomaterial from the absorption spectrum is about 3.57 eV [35]. Photoluminescence spectrum was obtained for ZrO_2 nanostructures synthesized at 250 °C for 24 h, in the wavelength range 300–500 nm with the excitation wavelength of 290 nm (inset (ii) of Fig. 7). The PL spectrum depicts a broad and prominent emission band centered at about 410 nm, which can be attributed to violet emission [13]. The species and densities of luminescence of the material control the emission peak position and strength. The intensity enhancement of UV emission at room temperature can be achieved by high crystal quality and quantum confinement in nanostructures. The broad emission band in the UV region is attributed to the singly ionized oxygen vacancies in ZrO_2 nanostructure. Hence, UV emission can arise as a result of the radiative recombination of a photo-generated hole with an electron occupying the oxygen vacancy [34]. The wide-band gap oxide nanostructures like ZrO_2 with short-wavelength PL emission can find application in light emitting devices.

4. Conclusions

ZrO_2 nanostructures were synthesized by hydrothermal route using zirconium salt as the starting material. Surface morphology analysis confirms the synthesis of nanobars and nanodiscs at various hydrothermal treatment conditions. XRD, HRTEM and SAED studies show that the synthesized ZrO_2 product is a pure monoclinic phase. Raman scattering spectra are analyzed and the Raman bands are assigned to various phonon vibration modes corresponding to the m-ZrO_2. The present technique provides an efficient route for the synthesis of m-ZrO_2 nanostructures with controlled morphology, high purity, uniform composition and high crystallinity. UV–vis spectrum shows a sharp absorption peak centered at about 292 nm and optical band gap of 3.57 eV is determined from the spectrum. PL spectrum shows a broad emission peak with maximum at 410 nm which can be assigned to violet emission. ZrO_2 nanostructures with wide-band gap and short-wavelength luminescence emission can serve as a good luminescent material for photonic applications.

Acknowledgements

This work was supported by a grant from National Science Foundation (DMR-0548061) to W.Z. Li. Raman studies were supported by grants from National Science Foundation (DMR-0231291) and Air Force (212600548) to S. K. Saxena. We would like to thank Dr. Jianmin Xu and Dr. Roger M. Leblanc for their help with the UV–vis and PL experiments.

References

[1] S. Park, J.M. Vohs, R.J. Gorte, Direct oxidation of hydrocarbons in a solid-oxide fuel cell, Nature 404 (2000) 265.
[2] Y.W. Li, D.H. He, Z.X. Cheng, C.L. Su, J.R. Li, M.J. Zhu, Effect of calcium salts on isosynthesis over ZrO_2 catalysts, Mol. Catal. A 175 (2001) 267.
[3] E.C. Subbarao, H.S. Maiti, Science and technology of zirconia, Adv. Ceram. 24 (1988) 731.
[4] Q. Zhang, J. Shen, J. Wang, G. Wu, L. Chen, Sol–gel derived ZrO_2–SiO_2 highly reflective coatings, Int. J. Inorg. Mater. 2 (2000) 319.
[5] P.K. Wright, A.G. Evans, Mechanisms governing the performance of thermal barrier coatings, Curr. Opin. Solid State Mater. Sci. 4 (1999) 25.
[6] C. Piconi, G. Maccauro, Zirconia as a ceramic biomaterial, Biomaterials 20 (1999) 1.
[7] P. Salas, E.D. Rosa-Cruz, L.A. Diaz-Torres, V.M. Castaño, R. Melèndrez, M. Barboza-Flores, Monoclinic, ZrO_2 as a broad spectral response thermoluminescence UV dosemeter, Radiat. Meas. 37 (2003) 187.

[8] S. Somiya, N. Yamamoto, H. Yanagina, Science and Technology of Zirconia III, American Ceramic Society, Westerville, OH, vol. 24A and 24B, 1988.
[9] G. Li, W. Li, M. Zhang, K. Tao, Characterization and catalytic application of homogeneous nano-composite oxides ZrO_2–Al_2O_3, Catal. Today 93 (2004) 595.
[10] W.-H. Tuan, J.-R. Chen, C.-J. Ho, Critical zirconia amount to enhance the strength of alumina, Ceram. Int. 34 (2008) 2129.
[11] P. Gao, L.J. Meng, M.P. dos Santos, V. Teixeira, M. Andritschky, Study of ZrO_2–Y_2O_3 films prepared by rf magnetron reactive sputtering, Thin Solid Films 377 (2000) 32.
[12] R.H. French, S.J. Glass, F.S. Ohuchi, Y.-N. Xu, W.Y. Ching, Experimental and theoretical determination of the electronic structure and optical properties of three phases of ZrO_2, Phys. Rev. B 49 (1994) 5133.
[13] A. Emeline, G.V. Kataeva, A.S. Litke, A.V. Rudakova, V.K. Ryabchuk, N. Serpone, Spectroscopic and photoluminescence studies of a wide band gap insulating material: powdered and colloidal ZrO_2 sols, Langmuir 14 (1998) 5011.
[14] C.-H. Lu, H.-C. Hong, R. Jagannathan, Sol–gel synthesis and photoluminescent properties of cerium-ion doped yttrium aluminium garnet powders, J. Mater. Chem. 12 (2002) 2525.
[15] M.H. Huang, S. Mao, H. Feick, H. Yan, Y. Wu, H. Kind, E. Weber, R. Russo, P. Yang, Room-temperature ultraviolet nanowire nanolasers, Science 292 (2001) 1897.
[16] P.G. McCormick, T. Tsuzuki, J.S. Robinson, J. Ding, Nanopowders synthesized by mechanochemical processing, Adv. Mater. 13 (2001) 1008.
[17] J.L. Gole, S.M. Prokes, J.D. Stout, O.J. Glembocki, R. Yang, Unique properties of selectively formed zirconia nanostructures, Adv. Mater. 18 (2006) 664.
[18] W.-J. Lee, W.H. Smyrl, Zirconium oxide nanotubes synthesized via direct electrochemical anodization, Electrochem. Solid-State Lett. 8 (2005) B7.
[19] C. Shao, H. Guan, Y. Liu, J. Gong, N. Yu, X. Yang, A novel method for making ZrO_2 nanofibres via an electrospinning technique, J. Cryst. Growth 267 (2004) 380.
[20] J. Bao, D. Xu, Q. Zhou, Z. Xu, Y. Feng, Y. Zhou, An array of concentric composite nanostructure of metal nanowires encapsulated in zirconia nanotubes: preparation, characterization, and magnetic properties, Chem. Mater. 14 (2002) 4709.
[21] H. Xu, D.-H. Qin, Z. Yang, H.-L. Li, Fabrication and characterization of highly ordered zirconia nanowire arrays by sol–gel template method, Mater. Chem. Phys. 80 (2003) 524.
[22] S. Sōmiya, T. Akiba, Hydrothermal zirconia powders: a bibliography, J. Eur. Ceram. Soc. 19 (1999) 81.
[23] K. Byrappa, T. Adschiri, Hydrothermal technology for nanotechnology, Prog. Cryst. Growth Charact. Mater. 53 (2007) 117.
[24] Y.V. Kolen'ko, V.D. Maksimov, A.V. Garshev, V.A. Mukhanov, N.N. Oleynikov, B.R. Churagulov, Physicochemical properties of nanocrystalline zirconia hydrothermally synthesized from zirconyl chloride and zirconyl nitrate aqueous solutions, Russ. J. Inorg. Chem. 49 (2004) 1133.
[25] L. Kumari, W. Li, D. Wang, Monoclinic zirconium oxide nanostructures synthesized by a hydrothermal route, Nanotechnology 19 (2008) 195602.
[26] X. Jiao, D. Chen, L. Xiao, Effects of organic additives on hydrothermal zirconia nanocrystallites, J. Cryst. Growth 258 (2003) 158.
[27] J.C. Ray, R.K. Pati, P. Pramanik, Chemical synthesis and structural characterization of nanocrystalline powders of pure zirconia and yttria stabilized zirconia (YSZ), J. Eur. Ceram. Soc. 20 (2000) 1289.
[28] J.P. Chang, Y.-S. Lin, Dielectric property and conduction mechanism of ultrathin zirconium oxide films, Appl. Phys. Lett. 79 (2001) 3666.
[29] E. Anastassakis, B. Papanicolaou, I.M. Asher, Lattice dynamics and light scattering in hafnia and zirconia, J. Phys. Chem. Solids 36 (1975) 667.
[30] P.E. Quintard, P. Barbéris, A.P. Mirgorodsky, T. Merle-Méjean, Comparative lattice-dynamical study of the Raman spectra of monoclinic and tetragonal phases of zirconia and hafnia, J. Am. Ceram. Soc. 85 (2002) 1745.
[31] M. Ishigame, T. Sakurai, Temperature dependence of the Raman spectra of ZrO_2, J. Am. Ceram. Soc. 60 (1977) 367.
[32] B.-K. Kim, H. Hamaguchi, Mode assignments of the Raman spectrum of monoclinic zirconia by isotopic exchange technique, Phys. Status Solidi (b) 203 (1997) 557.
[33] P. Barberis, T. Merle-Méjean, P. Quintard, On Raman spectroscopy of zirconium oxide films, J. Nucl. Mater. 246 (1997) 232.
[34] H.Q. Cao, X.Q. Qiu, B. Luo, Y. Liang, Y.H. Zhang, R.Q. Tan, M.J. Zhao, Q.M. Zhu, Synthesis and room-temperature ultraviolet photoluminescence properties of zirconia nanowires, Adv. Funct. Mater. 14 (2004) 243.
[35] D. Ciuparu, A. Ensuque, G. Shafeev, F. Bozon-Verduraz, Synthesis and apparent bandgap of nanophase zirconia, J. Mater. Sci. Lett. 19 (2000) 931.